Photonic crystal enhanced fluorescence using a quartz substrate to reduce limits of detection

Anusha Pokhriyal,[1] Meng Lu,[2] Vikram Chaudhery,[3] Cheng-Sheng Huang,[3] Stephen Schulz,[2] and Brian T. Cunningham[3,4,*]

[1]*Dept. of Physics, University of Illinois at Urbana-Champaign, Urbana, Illinois, USA*
[2]*SRU Biosystems, 14-A Gill St., Woburn, Massachusetts, 01810, USA*
[3]*Dept. of Electrical and Computer Engineering, University of Illinois at Urbana-Champaign, Urbana, Illinois, USA*
[4]*Dept. of Bioengineering, University of Illinois at Urbana-Champaign, Urbana, Illinois, USA*
**bcunning@illinois.edu*

Abstract: A Photonic Crystal (PC) surface fabricated upon a quartz substrate using nanoimprint lithography has been demonstrated to enhance light emission from fluorescent molecules in close proximity to the PC surface. Quartz was selected for its low autofluorescence characteristics compared to polymer-based PCs, improving the detection sensitivity and signal-to-noise ratio (SNR) of PC Enhanced Fluorescence (PCEF). Nanoimprint lithography enables economical fabrication of the subwavelength PCEF surface structure over entire 1x3 in^2 quartz slides. The demonstrated PCEF surface supports a transverse magnetic (TM) resonant mode at a wavelength of λ = 632.8 nm and an incident angle of θ = 11°, which amplifies the electric field magnitude experienced by surface-bound fluorophores. Meanwhile, another TM mode at a wavelength of λ = 690 nm and incident angle of θ = 0° efficiently directs the fluorescent emission toward the detection optics. An enhancement factor as high as 7500 × was achieved for the detection of LD-700 dye spin-coated upon the PC, compared to detecting the same material on an unpatterned glass surface. The detection of spotted Alexa-647 labeled polypeptide on the PC exhibits a 330 × SNR improvement. Using dose-response characterization of deposited fluorophore-tagged protein spots, the PCEF surface demonstrated a 140 × lower limit of detection compared to a conventional glass substrate.

OCIS codes: (050.5298) Photonic crystal; (180.2520) Fluorescence microscopy; (110.3960) Nanolithography.

References and links

1. J. R. Lakowicz, *Principles of Fluorescence Spectroscopy*, 3rd ed. (Springer, 2006), p. 954.
2. J. B. Pawley, ed., *Handbook of biological confocal microscopy*, 3rd ed. (J. Biomed. Opt., 2008), Vol. 13.
3. D. Axelrod, "Total internal reflection fluorescence microscopy in cell biology," Traffic **2**(11), 764–774 (2001).
4. F. Helmchen, and W. Denk, "Deep tissue two-photon microscopy," Nat. Methods **2**(12), 932–940 (2005).
5. J. Shendure, and H. Ji, "Next-generation DNA sequencing," Nat. Biotechnol. **26**(10), 1135–1145 (2008).
6. P. O. Brown, and D. Botstein, "Exploring the new world of the genome with DNA microarrays," Nat. Genet. **21**(1 Suppl), 33–37 (1999).
7. R. R. Koenen, and C. Weber, "Therapeutic targeting of chemokine interactions in atherosclerosis," Nat. Rev. Drug Discov. **9**(2), 141–153 (2010).
8. E. L. Moal, E. Fort, S. Lévêque-Fort, F. P. Cordelières, M.-P. Fontaine-Aupart, and C. Ricolleau, "Enhanced fluorescence cell imaging with metal-coated slides," Biophys. J. **92**(6), 2150–2161 (2007).
9. L. C. Estrada, O. E. Martinez, M. Brunstein, S. Bouchoule, L. Le-Gratiet, A. Talneau, I. Sagnes, P. Monnier, J. A. Levenson, and A. M. Yacomotti, "Small volume excitation and enhancement of dye fluorescence on a 2D photonic crystal surface," Opt. Express **18**(4), 3693–3699 (2010).
10. A. Kinkhabwala, Z. Yu, S. Fan, Y. Avlasevich, K. Müllen, and W. E. Moerner, "Large single-molecule fluorescence enhancements produced by a bowtie nanoantenna," Nat. Photonics **3**(11), 654 (2009).
11. K. Tawa, H. Hori, K. Kintaka, K. Kiyosue, Y. Tatsu, and J. Nishii, "Optical microscopic observation of fluorescence enhanced by grating-coupled surface plasmon resonance," Opt. Express **16**(13), 9781–9790 (2008).

#136118 - $15.00 USD Received 6 Oct 2010; revised 5 Nov 2010; accepted 6 Nov 2010; published 11 Nov 2010

12. J. R. Lakowicz, "Radiative decay engineering: biophysical and biomedical applications," Anal. Biochem. **298**(1), 1–24 (2001).
13. S. Fan, and J. D. Joannopoulos, "Analysis of guided resonances in photonic crystal slabs," Phys. Rev. B **65**(23), 235112 (2002).
14. K. A. Willets, and R. P. Van Duyne, "Localized surface plasmon resonance spectroscopy and sensing," Annu. Rev. Phys. Chem. **58**(1), 267–297 (2007).
15. P. Anger, P. Bharadwaj, and L. Novotny, "Enhancement and quenching of single-molecule fluorescence," Phys. Rev. Lett. **96**(11), 113002 (2006).
16. H. Hori, K. Tawa, K. Kintaka, J. Nishii, and Y. Tatsu, "Influence of groove depth and surface profile on fluorescence enhancement by grating-coupled surface plasmon resonance," Opt. Rev. **16**(2), 216 (2009).
17. K. H. Drexhage, "Influence of a dielectric interface on fluorescence decay time," J. Lumin. **1-2**, 693–701 (1970).
18. E. Matveeva, Z. Gryczynski, I. Gryczynski, and J. R. Lakowicz, "Immunoassays based on directional surface plasmon-coupled emission," J. Immunol. Methods **286**(1-2), 133–140 (2004).
19. J. Malicka, I. Gryczynski, Z. Gryczynski, and J. R. Lakowicz, "DNA hybridization using surface plasmon-coupled emission," Anal. Chem. **75**(23), 6629–6633 (2003).
20. C. D. Geddes, and J. R. Lakowicz, "Fluorescence Spectral Properties of Indocyanine Green on a Roughened Platinum Electrode: Metal-Enhanced Fluorescence," J. Fluoresc. **12**(2), 121–129 (2002).
21. J. R. Lakowicz, "Radiative decay engineering 5: metal-enhanced fluorescence and plasmon emission," Anal. Biochem. **337**(2), 171–194 (2005).
22. N. Ganesh, W. Zhang, P. C. Mathias, E. Chow, J. A. N. T. Soares, V. Malyarchuk, A. D. Smith, and B. T. Cunningham, "Enhanced fluorescence emission from quantum dots on a photonic crystal surface," Nat. Nanotechnol. **2**(8), 515–520 (2007).
23. B. T. Cunningham, and L. L. Laing, "Microplate-based, label-free detection of biomolecular interactions: applications in proteomics," Expert Rev. Proteomics **3**, 271–281 (2006).
24. J. N. Winn, Y. Fink, S. Fan, and J. D. Joannopoulos, "Omnidirectional reflection from a one-dimensional photonic crystal," Opt. Lett. **23**(20), 1573–1575 (1998).
25. H. Němec, L. Duvillaret, F. Garet, P. Kuže, P. Xavier, J. Richard, and D. Rauly, "Thermally tunable filter for terahertz range based on a one-dimensional photonic crystal with a defect," J. Appl. Phys. **96**(8), 4072 (2004).
26. D. Neuschäfer, W. Budach, C. Wanke, and S.-D. Chibout, "Evanescent resonator chips: a universal platform with superior sensitivity for fluorescence-based microarrays," Biosens. Bioelectron. **18**(4), 489–497 (2003).
27. P. C. Mathias, N. Ganesh, W. Zhang, and B. T. Cunningham, "Graded Wavelength One-Dimensional Photonic Crystal Reveals Spectral Characteristics of Enhanced Fluorescence," J. Appl. Phys. **103**(9), 094320 (2008).
28. P. C. Mathias, H.-Y. Wu, and B. T. Cunningham, "Employing two distinct photonic crystal resonances for improved fluorescence enhancement," Appl. Phys. Lett. **95**(2), 3 (2009).
29. I. D. Block, L. L. Chan, and B. T. Cunningham, "Large-Area submicron replica molding of porous low-k dielectric films and application to photonic crystal biosensor fabrication," Microelectron. Eng. **84**(4), 603–608 (2007).
30. K. R. Hawkins, and P. Yager, "Nonlinear decrease of background fluorescence in polymer thin-films - a survey of materials and how they can complicate fluorescence detection in mTAS," Lab Chip **3**(4), 248 (2003).
31. M. B. Wabuyele, S. M. Ford, W. Stryjewski, J. Barrow, and S. A. Soper, "Single molecule detection of double-stranded DNA in poly(methylmethacrylate) and polycarbonate microfluidic devices," Electrophoresis **22**(18), 3939–3948 (2001).
32. S. D. Llopis, W. Stryjewski, and S. A. Soper, "Near-infrared time-resolved fluorescence lifetime determinations in poly(methylmethacrylate) microchip electrophoresis devices," Electrophoresis **25**(21-22), 3810–3819 (2004).
33. A. Pokhriyal, M. Lu, C. S. Huang, S. Schulz, and B. T. Cunningham, "Multi-color fluorescence enhancement from a photonic crystal surface," Appl. Phys. Lett. **97**(12), 3 (2010).
34. A. Piruska, I. Nikcevic, S. H. Lee, C. Ahn, W. R. Heineman, P. A. Limbach, and C. J. Seliskar, "The autofluorescence of plastic materials and chips measured under laser irradiation," Lab Chip **5**(12), 1348–1354 (2005).
35. G. A. Diaz-Quijada, R. Peytavi, A. Nantel, E. Roy, M. G. Bergeron, M. M. Dumoulina, and T. Veresa, "Surface modification of thermoplastics-towards the plastic biochip for high throughput screening devices," Lab Chip **7**(7), 856 (2007).
36. F. Baldinia, A. Carlonia, A. Giannettia, G. Porrob, and C. Tronoa, "An optical PMMA biochip based on fluorescence anisotropy: Application to C-reactive protein assay," Sens. Actuators B Chem. **139**, 5 (2008).
37. S. Y. Chou, P. R. Krauss, and P. J. Renstrom, "Imprint Lithography with 25-Nanometer Resolution," Science **272**(5258), 85–87 (1996).
38. S. Y. Chou, P. R. Krauss, and P. J. Renstrom, "Imprint of sub-25 nm vias and trenches in polymers," Appl. Phys. Lett. **67**(21), 3114 (1995).
39. C. M. S. Torres, ed., *Alternative Lithography*, 1 ed., Nanostructure Science and Technology (Springer, 2003), p. 425.
40. S. Y. Chou, P. R. Krauss, W. Zhang, L. Guo, and L. Zhuang, "Sub-10 nm imprint lithography and applications," J. Vac. Sci. Technol. B **15**(6), 2897 (1997).
41. A. K. Kodali, M. Schulmerich, J. Ip, G. Yen, B. T. Cunningham, and R. Bhargava, "Narrowband midinfrared reflectance filters using guided mode resonance," Anal. Chem. **82**(13), 5697–5706 (2010).

#136118 - $15.00 USD Received 6 Oct 2010; revised 5 Nov 2010; accepted 6 Nov 2010; published 11 Nov 2010

42. N. Ganesh, I. D. Block, P. C. Mathias, W. Zhang, E. Chow, V. Malyarchuk, and B. T. Cunningham, "Leaky-mode assisted fluorescence extraction: application to fluorescence enhancement biosensors," Opt. Express **16**(26), 21626–21640 (2008).
43. M. Colburn, S. C. Johnson, M. D. Stewart, S. Damle, T. C. Bailey, B. Choi, M. Wedlake, T. B. Michaelson, S. V. Sreenivasan, J. G. Ekerdt, and C. G. Willson, "Step and flash imprint lithography: a new approach to high-resolution patterning," in *Proc. SPIE*, 1999), 379–389.
44. P. Ruchhoeft, M. Colburn, B. Choi, H. Nounu, S. Johnson, T. Bailey, S. Damle, M. Stewart, J. Ekerdt, S. V. Sreenivasan, J. C. Wolfe, and C. G. Willson, "Patterning curved surfaces: Template generation by ion beam proximity lithography and relief transfer by step and flash imprint lithography," J. Vac. Sci. Technol. B **17**(6), 2965 (1999).
45. D. J. Resnick, W. J. Dauksher, D. Mancini, K. J. Nordquist, T. C. Bailey, S. Johnson, N. Stacey, J. G. Ekerdt, C. G. Willson, S. V. Sreenivasan, and N. Schumaker, "Imprint lithography for integrated circuit fabrication," J. Vac. Sci. Technol. B **21**(6), 2624 (2003).
46. W. J. Dauksher, K. J. Nordquist, D. P. Mancini, D. J. Resnick, J. H. Baker, A. E. Hooper, A. A. Talin, T. C. Bailey, A. M. Lemonds, S. V. Sreenivasan, J. G. Ekerdt, and C. G. Willson, "Characterization of and imprint results using indium tin oxide-based step and flash imprint lithography templates," J. Vac. Sci. Technol. B **20**(6), 2857 (2002).
47. D. J. Resnick, D. Mancinia, W. J. Daukshera, K. Nordquist, T. C. Bailey, S. Johnson, S. V. Sreenivasan, J. G. Ekerdt, and C. G. Willsonb, "Improved step and flash imprint lithography templates for nanofabrication," Microelectron. Eng. **69**(2-4), 412 (2003).
48. I. D. Block, P. C. Mathias, N. Ganesh, S. I. Jones, B. R. Dorvel, V. Chaudhery, L. O. Vodkin, R. Bashir, and B. T. Cunningham, "A detection instrument for enhanced-fluorescence and label-free imaging on photonic crystal surfaces," Opt. Express **17**(15), 13222–13235 (2009).
49. V. Chaudhery, M. Lu, A. Pokhriyal, C. S. Huang, S. Schulz, and B. T. Cunningham, "Optimization of instrumentation for photonic crystal enhanced fluorescence microscopy," Submitted to Opt. Express (2010).
50. V. Chaudhery, M. Lu, C. S. Huang, S. George, and B. T. Cunningham, "Photobleaching on photonic crystal enhanced fluorescence surfaces," J. Fluores. Accepted September (2010).

1. Introduction

Fluorescence has emerged as the most widely used imaging and detection technique in life science research, disease diagnostics, and genomic/proteomic research tools due to its excellent sensitivity and specificity as well as the low cost and flexibility of the method [1]. Detection of single fluorophores is becoming routine for techniques that can confine illumination to small volumes in order to avoid excitation of fluorescent tags or autofluorescent materials that are not confined to an assay surface. These techniques include confocal microscopy [2], total internal reflection microscopy (TIRF) [3], and two-photon excitation microscopy (TPEM) [4]. The ability to detect weak fluorescent signals above background autofluorescence is especially important for detection of biomolecular analytes that are present at very low concentrations (DNA sequencing [5], gene expression microarrays [6], and protein biomarker immunoassays [7]) and cell imaging. To maximize the sensitivity of the fluorescence technique, a variety of nano-patterned structures including metal coated slides, plasmonic gratings, 2D photonic crystals and nanoantenna, have been studied for the purpose of enhancing the fluorescence output [8–11]. Unlike confocal microscopy or TIRF microscopy, these approaches seek to use the nanostructure to enhance the electric field intensity experienced by the surface-bound fluorophores, so as to provide a "gain" mechanism that is not present upon an ordinary surface. Such surfaces have also been shown to incorporate additional signal enhancement mechanisms that include increased particle extinction coefficients, reduced fluorescence lifetimes, and directional emission [12–16]. An extensive literature has evolved since pioneering work in the field several decades ago [17–19] and numerous reviews exist summarizing recent progress [20,21].

While metal-based nanostructures primarily use surface plasmons to provide enhanced surface-bound electric fields, plasmon resonances provide limited field enhancement due to their low quality factor and losses in metal that occur at optical wavelengths. Further, fluorophore emission quenching occurs for molecules within <10 nm [21] of a metal surface, resulting in a requirement for spacer layers that have restricted wide adoption of plasmon-based approaches. Dielectric-based optical resonators are capable of providing a high quality factor, and therefore are capable of providing higher electric field enhancement. Dielectric

#136118 - $15.00 USD Received 6 Oct 2010; revised 5 Nov 2010; accepted 6 Nov 2010; published 11 Nov 2010

resonators, including PC surfaces [22], have been demonstrated not to quench fluorophores, while enabling direct illumination through their substrate due to their optical transparency.

A one dimensional surface PC structure comprised of a low refractive index periodic surface grating coated with a high refractive index dielectric thin film has been extensively studied due to its application as an optical filter, narrow bandwidth mirror, label-free biosensor and others [23–25]. Use of PC surfaces for fluorescence emission enhancement applications through the use of narrowband resonant modes at specific wavelengths has also been demonstrated. Electric fields associated with resonant reflection, confined within the PC and evanescent into the adjacent media are strongly enhanced with respect to the electric field of the external illumination source [26]. By spectrally aligning a PC resonant mode with the laser used to excite fluorescent dyes, one can achieve an increase in the emission intensity of the dye in comparison to the same fluorophore excited on a plain glass surface. This has an advantage of enhancing the fluorescence of molecules only close to the surface, while not enhancing fluorophore sources in bulk solution or within the device substrate. Previous publications have demonstrated the use of PCEF with the resonant mode spectrally overlapping the laser wavelength to excite fluorescent dyes [27], and, at normal incidence illumination, a PC with a resonant mode at λ = 632.8 nm producing a 60-fold magnification of cyanine-5 (Cy-5) signal compared to an ordinary glass substrate [28].

Our previous results with PCEF have been obtained using a polymer grating structure produced by the nanoreplica molding technique [29] on flexible plastic substrates. Fluorescent detection limits of PCs incorporating polymer materials has been limited by the fluorescence background (autofluorescence) signal produced by the plastic substrate and polymer grating. It is well known that plastic materials show significant autofluorescence when excited by near-UV or even visible radiation [30–32], with autofluorescence increasing as the illumination source photon energy is increased. This phenomena was demonstrated clearly in a recent publication, in which a PCEF surface designed for multiple excitation wavelengths (λ = 532 - 633 nm) showed best signal-to-noise sensitivity performance for longer excitation wavelengths, however the detection limit for short excitation wavelengths was limited by substrate autofluorescence [33]. Meanwhile, a great deal of research activity is directed towards developing new plastic substrates with lower autofluorescence [34–36]. PMMA, PDMS, Topas and Zeonex have been shown to have lower autofluorescence compared to other plastic materials and have been identified for potential applications in high throughput screening devices that rely on fluorescence detection. Despite these efforts, no polymer material provides autofluorescence comparable to quartz.

The use of quartz surfaces for PCEF applications has been limited by the requirement to produce surface structures with subwavelength dimensions over surface areas large enough to encompass entire DNA microarrays or protein microarrays, which are usually performed on substrates as large as standard microscope slides (1×3 in^2). Conventional lithography methods, such as e-beam lithography and DUV lithography, are either too expensive or low throughput to produce subwavelength structures over such large surface areas. In order to address this issue, “step-and-flash” nanoimprint lithography (NIL) tools (Molecular Imprints, Inc.) can be employed to fabricate subwavelength grating structures on quartz substrates [37–40]. Step-and-flash imprint lithography (SFIL) has been successfully demonstrated for hard drive disks, LEDs, and CMOS manufacturing. SFIL is capable of producing patterns with feature sizes less than 20 nm. In the SFIL process, a template with a pre-defined pattern is pressed into UV-curable liquid over a substrate. Once exposed to UV light, the liquid is cured, and after separation, a replica of the pattern on the template is imprinted into the solidified polymer surface. A step and repeat procedure is used to replicate the pattern over the entire substrate surface. After SFIL patterning, reactive ion etching (RIE) is used to transfer the imprinted pattern into the substrate. Using this approach, we have fabricated one dimensional grating structure with a period of 400 nm upon quartz wafers as large as 8 inches in diameter.

#136118 - $15.00 USD Received 6 Oct 2010; revised 5 Nov 2010; accepted 6 Nov 2010; published 11 Nov 2010

In this paper we demonstrate and characterize a quartz-based PCEF substrate produced using SFIL nanoimprint lithography. The device design is described in Section 2, and the fabrication process is detailed in Section 3. Section 4 characterizes the performance of the PCEF surface, demonstrating low autofluorescence and strong fluorescence signal enhancement when the device is illuminated by a λ = 632.8 nm laser at the resonant angle. An enhancement factor as high as 7500 × was achieved. Using the PCEF surface, the detection of dye labeled peptide is shown in Section 5. The surface is capable of lowering the detection limit of this analyte by a factor of 140 × .

2. PCEF surface design

The PCEF structure supports resonant modes at a specific combination of wavelength and angle of incidence [41]. The near field intensity associated with the resonant modes is strongly enhanced with regard to the field intensity of excitation light. The enhanced near field on the surface of the substrate can amplify the emission intensity from target fluorescent molecules. A cross-sectional diagram (not to scale) of the PCEF surface that was fabricated is shown in Fig. 1. The subwavelength grating is formed on the surface of the quartz with a refractive index of $n_{sub} = 1.456$. A layer of a high refractive index ($n_{TiO2} = 2.35$) dielectric material with a specified thickness (t_{TiO2}), is subsequently deposited over the grating structure. The periodic modulation of the grating, which satisfies the second order Bragg condition, allows for phase-matching of an externally incident beam into resonant modes. The high refractive index layer functions as a light confinement layer that supports and intensifies electric field that extends from the device surface into the surrounding medium. The wavelength, angle of incidence, bandwidth, and efficiency of the PCEF surface is determined by the geometry of the structure as described in previous publications [22,42]. By adjusting the PC geometric parameters, including the grating period (Λ), grating depth (d), duty cycle (f), thickness and refractive index of the dielectric coating, a PCEF surface can be designed to efficiently interact with the absorption and emission spectra of specific fluorescent dye molecules.

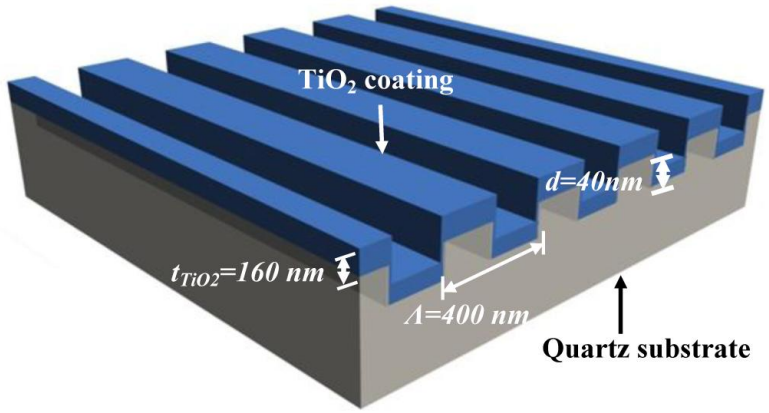

Fig. 1. Schematic diagram of PCEF surface on a quartz substrate. The subwavelength grating structure is etched into the quartz substrate and a high refractive index dielectric (TiO_2) film is coated on top of the grating as a light confinement layer.

In this study, the PCEF surface was designed to enhance the emission from fluorescent dyes which have an absorption band at λ_{ex} = 632.8 nm and an emission band near λ_{em} = 690 nm. The detection instrument is equipped with a HeNe laser (λ = 632.8 nm) as the excitation source and an emission filter with a center wavelength of 690 nm and bandwidth of 40 nm. A PC structure usually supports two orthogonal modes: transverse electric (TE) polarized and transverse magnetic (TM) polarized. Compared to TE modes, the resonant modes associated with TM polarization have higher *Q*-factor, resulting in stronger field intensity near the device surface. Therefore, the PCEF surface was designed to have one TM mode at λ_{ex} = 632.8 nm

#136118 - $15.00 USD Received 6 Oct 2010; revised 5 Nov 2010; accepted 6 Nov 2010; published 11 Nov 2010

which spectrally matches with the excitation laser wavelength for near field enhancement, resulting in "enhanced excitation." Meanwhile, aother TM mode at λ_{em} = 690 nm, which spectrally overlaps with the pass band of the emission filter was used to direct the emitted photons towards the detection optics to obtain an "enhanced extraction" effect [42]. Fluorescent output efficiently coupled into the second TM mode exhibits an angle dependent emission. In most fluorescent microscopes and confocal fluorescent scanners, the collection optics are placed perpendicular to the substrate surface. In order to direct the emitted photons toward the collection optics, the TM mode (λ_{em} = 690 nm), which is responsible for enhanced extraction, is designed with a resonant angle θ_{em} = 0°.

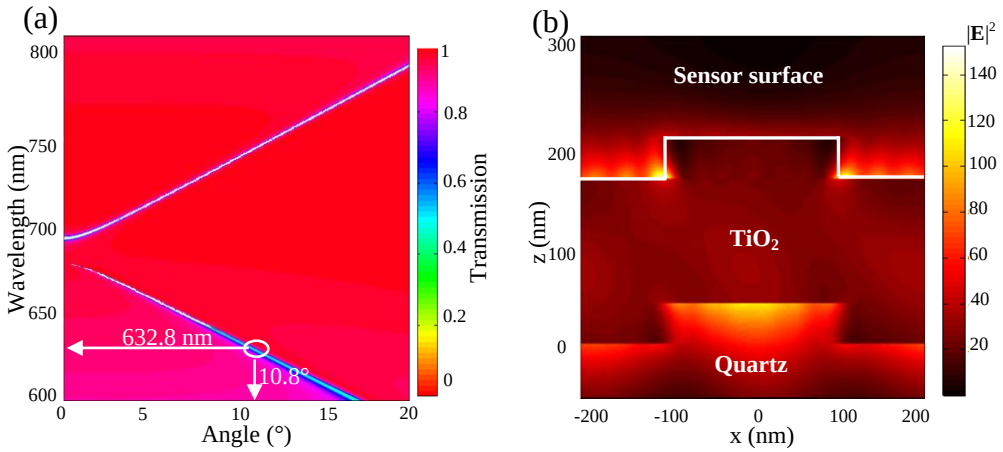

Fig. 2. (a) RCWA simulated dispersion diagram for the PC used in this study. Resonance for the enhanced excitation for the TM mode is at ~10.8°(b) Simulated near field distribution at λ = 632.8 nm (normalized to the intensity of the incident field).

A commercially available electromagnetic simulation package (DIFFRACTMOD, RSoft Design) was used to aid the design of the PCEF surface with multiple TM modes with precisely defined wavelength/angle coupling conditions. This simulation tool implements rigorous coupled-wave analysis (RCWA) and can output diffraction efficiency in terms of wavelength or field distribution in the computation domain at a specific wavelength. For the PC structure, transmission efficiency minima (or reflection efficiency maxima) in the calculated spectra was used to identify the resonant mode. RCWA simulation results stipulated the use of a structure with a period of Λ = 400 nm, grating depth of d = 40 nm, duty cycle f = 50%, and TiO_2 thickness of t_{TiO2} = 160 nm. For this design, the transmission efficiency of the TM resonant mode was calculated in the wavelength range of 600< λ<800 nm and the incident angle was varied from 0° <θ< 20°. By plotting transmission spectra, Fig. 2(a) presents the photonic band diagram of the PCEF surface shown in Fig. 1. From the photonic band diagram, a resonant angle of θ_{ex} = 10.8° corresponds to a resonant wavelength of λ_{ex} = 632.8 nm for enhanced excitation. Figure 2(b) shows the spatial distribution of the simulated near-field electric field intensity (normalized to the intensity of incident field) within one period of the PC structure for resonant wavelength λ_{ex} = 632.8 nm and resonant angle of θ_{ex} = 10.8°. The influence of the resonance phenomenon on the resulting near-fields is clearly manifested in the electric field intensity. At θ_{em} = 0°, the upper band edge with λ_{em} = 690 nm is used for enhanced extraction (shown in Fig. 2(a)). The enhanced extraction effect offers the possibility of efficiently collecting fluorescent emission using a low numerical aperture (NA) lens. Our fluorescence detection instrument is installed with a microscope objective with NA = 0.1. This low NA objective can only accept light within an angular acceptance cone of 5.7° and thus offers additional benefit in the fluorescent signal detection. Since the designed excitation angle θ_{ex} = 10.8° is much larger than 5.7°, the excitation beam

#136118 - $15.00 USD Received 6 Oct 2010; revised 5 Nov 2010; accepted 6 Nov 2010; published 11 Nov 2010

will not be visible to the detection system. This feature of the detection instrument is extremely important for obtaining low background intensity measurements because a small fraction of excitation light coupled into detection optics can pass through the emission filter, thus compromising signal-to-noise performance.

3. PCEF surface fabrication

The subwavelength grating surface (1×3 in^2) was prepared by nano-imprint lithography using the SFIL process, performed on a commercially available tool (Molecular Imprint Inc. Imprio-55) [43–45]. The template used for the imprint was patterned with the grating structure within an area of 9×9 mm^2 by e-beam lithography and RIE [46,47]. Ultra-low autofluorescence quartz wafers (4 inch diameter) were chosen as an imprint substrate. Before imprinting, the quartz wafers were pre-cleaned in Piranha solution for 1 hr. and then washed in Spin-Rinse-Dry (SRD 19A Verteq Process Systems Development) for 1 hr. to remove particles.

Details of the fabrication processes are illustrated in Fig. 3. For the purpose of planarization, the substrate was pre-coated with Transpin (Molecular Imprints Inc.) and hard baked for 60 sec. on a hotplate at 160 °C to produce a 60 nm thick film. As shown in Fig. 3(a), imprint resist (MonoMat, Molecular Imprint Inc.) was dispensed onto the substrate. The dispense pattern and volume was precisely controlled so as to fill the template shape with minimum protrusions out of the imprint area and to have a uniform base layer thickness. The template was then slowly pressed against the dispense pattern on the substrate for 70 sec. followed by UV exposure to cure the MonoMat for 20 sec. to produce a solidified polymer. After UV cure, the template was released from the imprint resist by applying a pulling force. After the imprint, the grating pattern was transferred into imprint resist with a base layer thickness of ~60 nm. The release of the template from the imprint resist after the UV exposure was facilitated by pre-treatment of the template with an anti-adhesion monolayer (RelMat, Molecular Imprints, Inc.). This imprint process was repeated in a series of die within an x-y grid to cover the entire quartz wafer surface.

After the imprint, RIE was used to transfer the imprinted pattern into the quartz substrate. In order to improve fidelity, the imprinted wafer was coated with a silicon- or silixane-containing polymer layer (SilSpin, Molecular Imprint Inc.) at 3,000 rpm and baked on a hotplate at 200 °C for 90 sec. (Fig. 3(d)). As shown in Fig. 3(e), during oxygen RIE, the Silspin surface forms a SiO_2 layer which functions as a high selectivity mask for the etching of MonoMat and Transpin. To etch back SilSpin, RIE was performed with 30 sccm of CHF_3 and 2.7 sccm of O_2 at a chamber pressure of 35 mTorr. This etching step is precisely timed so as to expose imprint resist at the end of the SilSpin etch. Using Silspin as an etching mask, the imprint resist and TranSpin layers were etched by an anisotropic RIE with 12 sccm of Ar and 2.7 sccm of O_2 in order to expose the quartz substrate. Finally, a RIE with CF_4 was used to transfer the grating pattern into the quartz wafer. After this, the wafer was cleaned by Piranha to remove all residues of the imprint polymers. The substrate was then cut into two standard microscope slides (1×3 in^2) by a dicing saw (600 Series, Disco Corporation). The RF sputter (PVD 75, Kurt J. Lesker) with a ceramic TiO_2 target was used to coat 160 nm of TiO_2 on top of the imprinted grating structure.

#136118 - $15.00 USD Received 6 Oct 2010; revised 5 Nov 2010; accepted 6 Nov 2010; published 11 Nov 2010

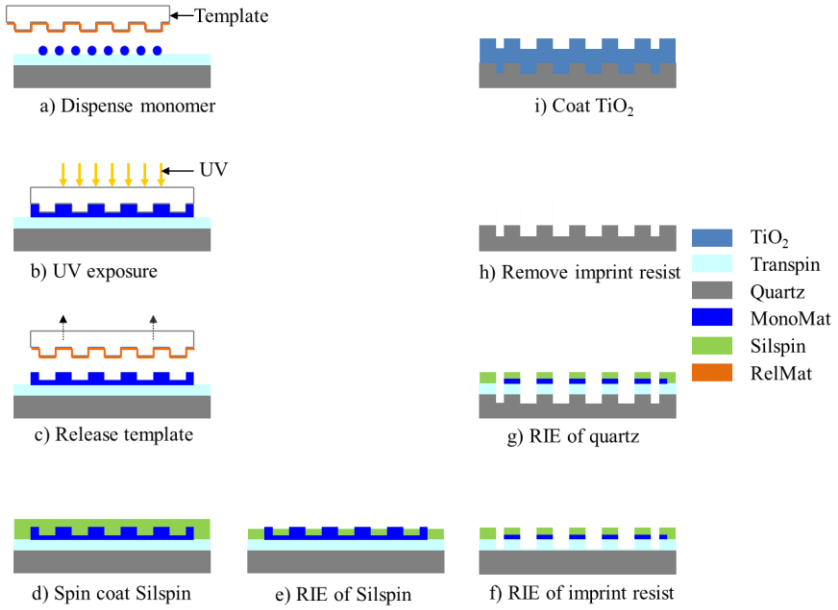

Fig. 3. Schematic diagram of the fabrication procedure: (a) The process begins with a dispense pattern of MonoMat on a planarized quartz wafer; (b) The template is pressed against the dispense pattern and then UV cured; (c) The template is pulled away from the solidified grating pattern; (d) A layer of Silspin is spin coated onto the patterned surface; (e) RIE of SilSpin to expose imprint resist; (f) RIE of the imprint resist to expose the quartz surface; (g) RIE of quartz to transfer the pattern onto the wafer; (h) Piranha cleaning of the wafer to remove the imprint resist residues; (i) TiO_2 deposition onto the grating.

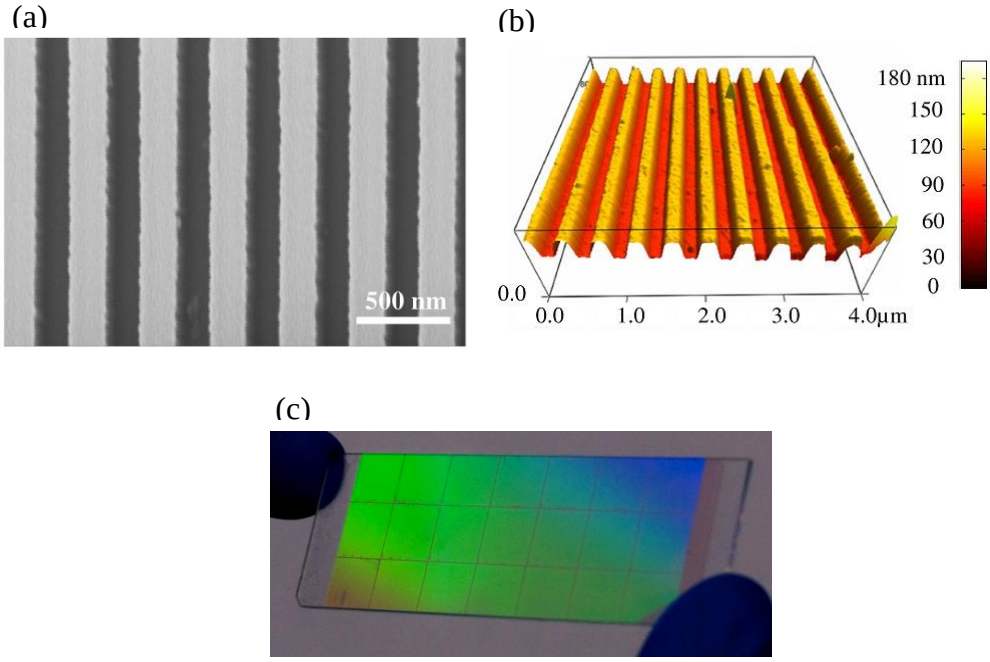

Fig. 4. (a) SEM image of the top view of the TiO_2 coated grating structure on quartz substrate; (b) AFM image of the PCEF surface showing the grating depth of 40 nm; (c) Photograph of the PCEF surface on 1 × 3 in^2 substrate.

#136118 - $15.00 USD Received 6 Oct 2010; revised 5 Nov 2010; accepted 6 Nov 2010; published 11 Nov 2010

A scanning electron microscope (SEM) image of the top view of the fabricated quartz grating is presented in Fig. 4(a). It is evident from the SEM image that the sidewalls of grating are free from debris and essentially vertical. An atomic force microscope surface profile of the imprinted structure after the TiO_2 deposition is shown in Fig. 4(b). The geometric dimensions (grating period of Λ = 402 nm and grating depth of d = 44 nm) match closely with the design dimensions. Figure 4(c) shows a photograph of the PCEF surface in a standard 1 × 3 in^2 microscope slide format with 21 imprint replicas. The slides show excellent uniformity across the entire area. Capable of accurately reproducing subwavelength feature sizes over a large range, the NIL process reported here is well suited for mass production of PCEF surfaces.

4. Device characterization

Several experiments were conducted to characterize the transmission spectrum, autofluorescence intensity, enhanced excitation, and directional emission properties of the PC sensor.

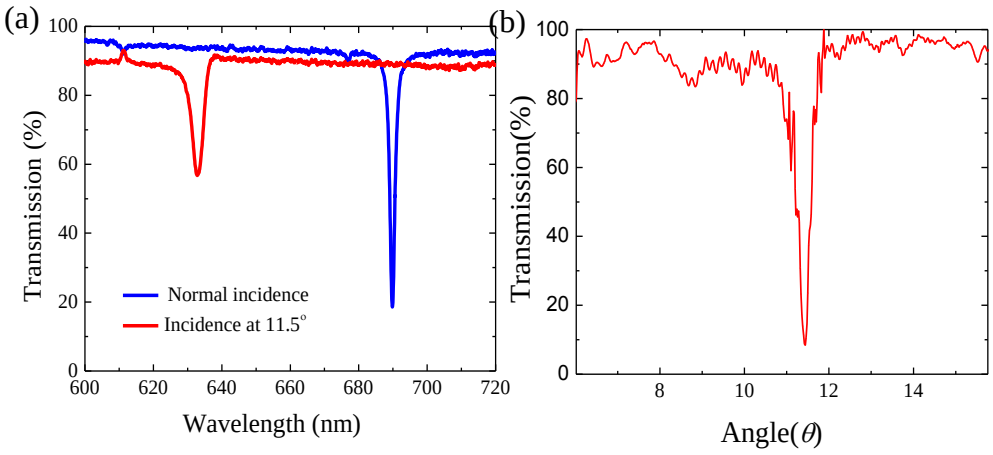

Fig. 5. (a) Wavelength transmission spectrum; (b) Angle transmission spectrum at the excitation wavelength λ = 632.8nm.

4.1 Transmission spectrum of PC sensor

In order to measure the resonant wavelength and angle of the fabricated device, the wavelength transmission spectra were collected by illuminating the PC with a TM polarized broadband light from a halogen lamp and analyzing the transmitted spectrum, using a spectrometer (HR2000, OceanOptics) coupled to an optical fiber. The blue curve in Fig. 5(a) shows the transmission spectrum taken at normal incidence (θ = 0°), with full width at half maximum (FWHM) of ~1 nm. Designed as a mode for enhanced extraction, this mode has a resonant wavelength of λ_{em} = 689.7 nm which entirely overlaps with the pass band of the emission optical filter of the detection instrument. In Fig. 5(a), the red curve shows the transmission spectrum at the incidence angle of θ_r = 11.4°. At this angle, the resonant wavelength exactly matches the excitation laser wavelength of 632.8 nm with FWHM of ~4 nm. Compared to the normal incidence case, off-normal resonance modes are more sensitive to beam divergence. Since the setup here used a fiber coupled broadband light, the incidence beam at 11.4°diverged reducing the coupling efficiency and leading to the poor contrast in Fig. 5(a). The resonant angle (θ_r) was also identified by illuminating the device with a TM polarized HeNe laser (35 mW), tuning the angle of incidence, and recording the transmitted light intensity. The illumination spot size was ~3 mm in diameter. The measured angle spectrum is shown in Fig. 5(b) with $FWHM_\theta$ = 0.3°. To fully take advantage of the enhanced excitation effect, the angle of incidence needs to be well tuned to efficiently couple the

#136118 - $15.00 USD Received 6 Oct 2010; revised 5 Nov 2010; accepted 6 Nov 2010; published 11 Nov 2010

excitation light into the resonant mode at θ_r = 11.4°. A PC enhanced fluorescence microscope (PCEFM) developed by our group and described fully in a previous publication [48], was used to perform the angle tuning. When the illumination angle was tuned to θ_r, the fluorescent images were taken.

4.2 Autofluorescence characterization of the quartz PCEF surface

Reducing the fluorescent emission from the sensor substrate is critical for the detection of fluorescent tags present at low concentration. The flame-fused quartz substrate (University Wafer) used in this experiment exhibits ultra-low autofluorescence when excited by a red laser source. The autofluorescence level of the quartz substrate was compared to a commercial glass slide and a PCEF surface fabricated by replica molding on a plastic substrate [17]. Glass slides and the polymer-based PC surfaces are currently the most commonly used substrates for surface-based fluorescent assays. The polymer-based PC and quartz-based PC have resonant modes at λ_{ex} = 632.8 nm with the resonance angle at 13° and 11.4°, respectively.

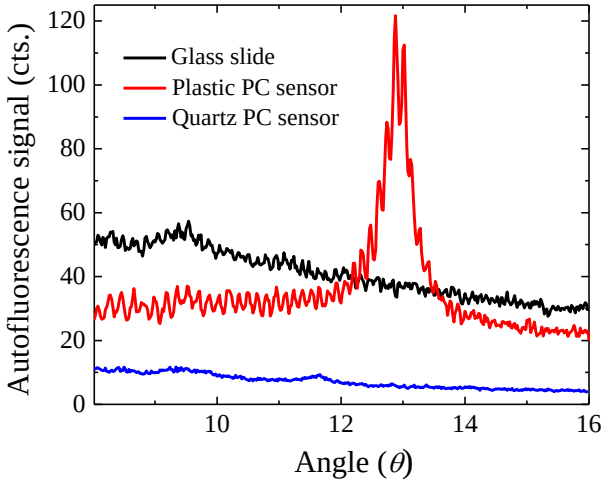

Fig. 6. Autofluorescne intensity from a normal glass slide, a plastic-based PCEF surface, and a quartz-based PCEF surface measured using the PC fluorescent microscope under identical measurement settings.

Before the measurements, all devices were cleaned in oxygen plasma for 5 min. to remove possible organic contaminations. All devices were measured using the fluorescent detection setup described in [48]. A 35 mW HeNe laser was employed as the excitation source; a 20 × objective (NA = 0.4) was used to collect the autofluorescnece signal; the λ = 690 ± 20 nm emission filter was applied to block laser light from reaching the CCD camera in the detection instrument. All the images were taken at 1.2 sec integration time. Figure 6 shows the autofluorescence for the glass slide, polymer-based PC and the quartz-based PC for illumination angles between 0° and 16°. The glass slide sample showed a nearly constant autofluorescence signal of ~50 cts. The polymer-based PC sensor exhibited strong background fluorescence near the resonant angle of 13° due to PC enhancement of autofluorescent material in contact with the resonant mode. The quartz-based PC showed background fluorescence as low as 15 cts., which is 15 times lower than the polymer-based PC on-resonance and 5 times lower than the glass slide. In Fig. 6, we observe that the quartz based PC did not show a peak in autofluorescence corresponding to the on-resonance condition. We understand that this is due to the lack of autoflourescence coming from the quartz substrate. The PC on-resonance excitation will only enhance signal coming from sources within ~100-

#136118 - $15.00 USD Received 6 Oct 2010; revised 5 Nov 2010; accepted 6 Nov 2010; published 11 Nov 2010

150 nm from the device surface. Hence, even on-resonance, this enhancement in the autofluorescence signal is hard to distinguish from the noise in the PCEFM.

4.3 Enhanced excitation and extraction

A simple testing scheme was developed to characterize the signal enhancement capability of the PCEF surface. A fluorescent dye (LD-700, Exciton, Inc) with a peak absorption wavelength of 647 nm and a peak emission wavelength of 673 nm was doped in SU-8 (n_{SU8} = *1.58*) and spin-coated onto the PC surface [9]. The SU-8 host medium was prepared by mixing SU-8 2000.5 with SU-8 thinner (Microchem Corporation) at a volume ratio of 1:12. The LD-700 dye molecules were first dissolved in methanol at 10^{-6} M (538 ng/ml) and then mixed with diluted SU-8 solution at a volume ratio of 1:2. The LD-700 doped SU-8 solution was then spin coated onto the PC surface at 5000 rpm for 30 sec and then air dried. The coated film thickness was measured as ~50 nm by ellipsometer. The deposition of dye-doped SU-8 film causes a resonant angle shift of 3.5° due to the shift in the resonant wavelength, as the film slightly increases the effective refractive index of the resonant mode.

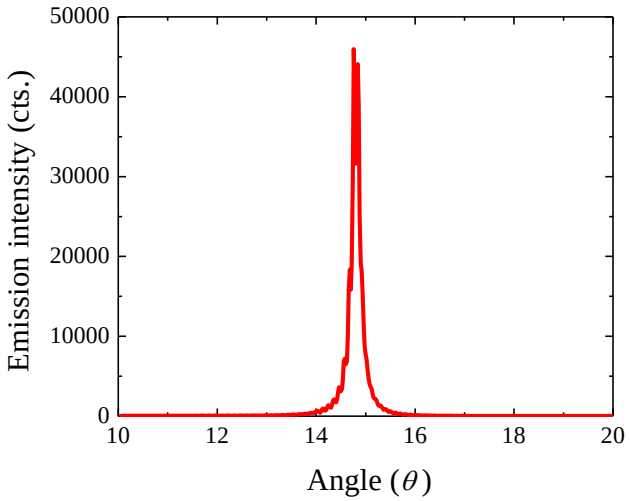

Fig. 7. Fluorescence output as a function of angle of incidence for a ~50 nm film of dye-doped polymer applied directly to the PCEF surface.

The dye/polymer coated PCEF surface was tested using the PCEF microscope instrument, which illuminates the surface from beneath the structure with collimated light that can be swept rapidly through a range of incident angles [48,49]. The system incorporates a TM-polarized HeNe laser, while the emission is collected by a 0.1 NA objective (positioned above the device), filtered by a 690 ± 20 nm emission filter, and measured by an electron multiplied CCD (EMCCD) camera. By varying the angle of incidence from 10° to 20° in increments of 0.02°, the emission intensity was recorded as shown in Fig. 7. The images were taken with an integration time of 30 msec. At the resonant angle (θ_r = 14.88°), the measured fluorescent intensity is ~45,000 cts.. Off-resonance illumination (θ = 20°), resulted in a fluorescence signal of only ~45 cts.. The enhancement factor of the PCEF surface was calculated by subtracting the background from the signals and dividing the on-resonance net signal by the off-resonance net signal. An enhancement factor of 1500 × was obtained, representing the effects of enhanced excitation only.

Using the same sample, the enhanced extraction effect was also studied with PCEF microscope, the LD-700 coated PC was illuminated at an off-resonance angle (θ = 20°) with the TM polarized HeNe laser. To characterize the enhanced extraction effect, an integration time of 1.2 sec was used for the EMCCD camera because the fluorescent intensity from the

#136118 - $15.00 USD Received 6 Oct 2010; revised 5 Nov 2010; accepted 6 Nov 2010; published 11 Nov 2010

glass control was too low to be detected when integration times of <100 msec were used. A background subtracted off-resonance fluorescent intensity of 10940 cts. was collected by the NA = 0.1 objective for the PCEF surface. A glass control with LD-700 coated at the same concentration under similar conditions was also studied using the PCEF microscope under the same conditions. A background subtracted fluorescent intensity of 2050 cts. was collected by the NA = 0.1 objective for the glass control. The ratio of background subtracted off-resonance signal and the background subtracted glass control signal gives the extraction enhancement factor of the device. From the above data, the PCEF surface gave a factor of 5 × for enhanced extraction.

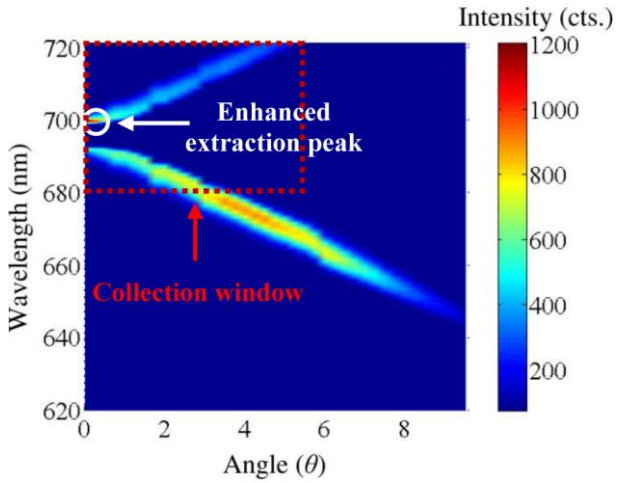

Fig. 8. Angle-resolved fluorescence measurement on the quartz PCEF surface.

A combined enhancement factor, (defined as the product of the enhanced excitation and the enhanced extraction factors) of 7500 × was calculated for the device for the given concentration of LD-700. This enhancement factor represents the maximum achievable enhancement that can be obtained when fluorescent material is allowed to fill a ~50 nm thick volume that conforms to the corrugated PC surface, with no spacer materials between the fluorescent layer and the PC surface for the demonstrated design of the PCEF surface. The addition of the ~50 nm SU8 layer results in a 10% increase of the Q-factor of the PC and thus increases the enhancement factor by ~10%. Addition of biomolecular layers to the bare PC results in approximately the same effect. As we will show, detection of fluorescent-tagged biomolecules results in lower total enhancement factor, as fractional monolayers of proteins with ~1 dye molecule each do not fill the evanescent field volume with dye as efficiently as the SU8-doped layer.

A short study was done to look at the enhanced extraction effect on the PC by looking at the angle and wavelength-resolved emission plot of the fluorescence. The measurement setup designed to collect and analyze the fluorescent intensity as a function of the angle of collection comprised of an optical fiber mounted on a collimator with the acceptance range for the angles between 0° and 0.3°. In order to show that enhanced extraction only depends upon the emission peak of the fluorophore, a different dye, LDS-720 (λ_{abs} = 529 nm, λ_{em} = 699 nm) was used as the flourophore doped in SU8 film. A diode pumped green laser (λ = 532 nm; 300 mW) was used as the excitation light source. The green laser beam was used to illuminate the sample surface at a fixed angle of incidence (θ = 0°) and the dye emission was collected by an optical fiber mounted with a collimator. The emission spectra were sampled and analyzed by the spectrometer with exit angles between 0° to 9° at increments of 0.25°. Figure 8 shows an angle and wavelength-resolved emission plot of the fluorescence as collected by rotating the fiber probe relative to device surface. The detection window of the PCEF microscope was defined as 680<λ<720 nm and an angle range of 0° to 5.7°, corresponding to the collection

#136118 - $15.00 USD Received 6 Oct 2010; revised 5 Nov 2010; accepted 6 Nov 2010; published 11 Nov 2010

window of the NA = 0.1 collection lens used in our microscope (as labeled in Fig. 8). Within this window, 77% of the fluorescence is gathered, which is ~9 × higher than the fluorescent intensity that is gathered by the same experiment performed upon a conventional glass substrate. This factor was calculated by assuming that the fluorescent emission on a glass is spherically symmetric. Also, one can see a strong peak at $\lambda = 690$ nm at an exit angle of 0°. As mentioned previously, this TM peak is used to couple the emission of the fluorescent molecules and direct it towards the collection optics.

5. Detection of dye labeled polypeptide

In order to demonstrate the enhancement in the SNR and lowering of the limit of detection of the analytes on the PCEF surface in the context of a multispot microarray assay, a detection experiment using a dye-labeled protein was performed. Spots of dye-labeled polypeptide with a range of dye concentrations were applied directly to the PCEF surface and a glass surface, and the fluorescence output of spots on each surface were compared in a dose-dependent manner. Both the PC surface and the glass slide were pre-cleaned with O_2 plasma for 3 min. and were further cleaned by sonication in acetone, isopropanol and deionized (DI) water and then dried under a nitrogen stream. Poly(Lys, Phe) conjugated with Alexa-647 (Invitrogen) at a range of concentrations was spotted onto the slides by a piezoelectric dispenser (Piezorray, Perkin Elmer) with a center-to-center separation of 500 μm and a spot radius of ~200 μm. After an incubation period of 50 min, the devices were washed by gently dipping them in DI water for 60 sec. Fluorescent images of the spots were then taken using the PCEF microscope. The Alexa-647 labeled polypeptide (PPL-Alexa 647) spots were excited with the TM polarized HeNe laser at the angle of incidence $\theta = 11.4°$ and the emission was collected with a NA = 0.1 objective, as described previously. The measured images were analyzed by image processing software (ImageJ). The net fluorescence intensity was calculated by averaging spot intensities over the 9 replicate spots minus the local background intensity.

The fluorescence images for both the PC and glass slide for four consecutive concentrations are shown side-by-side in Fig. 9 (images were plotted using the same grey scale). An integration time of 30 msec was used for all the images taken by the PCEF microscope. Representative line profiles generated by extracting fluorescence intensities from a single line of pixels through spots on the PC and glass images are also shown in Fig. 9. For the concentration of 30μg/ml, the spots on the PC saturate at 65535 cts. (saturation limit of the CCD), while for glass slide the signal is 3150 cts.. For the concentration of 9.9μg/ml, the signal on the glass slide has already decreased to 80 cts. compared to the PC at 60000 cts.. This profile clearly illustrates amplification of the emission signal from the fluorophore on the PC surface. Table 1 summarizes the measured fluorescence enhancement for the four consecutive concentrations of PPL-Alexa 647 spotted on the quartz-based PC and separates the individual effects of enhanced excitation (measured as the ratio of fluorescence intensities for the PC illuminated on- versus off-resonance) and enhanced extraction (measured as the ratio of fluorescence intensities for the PC off-resonance versus the glass slide control). The trend of decreasing enhanced excitation for higher spot concentration arises because the optimal resonance angle for the 3.3 μg/ml spots was used as the illumination angle for the on-resonance case for the spots of every concentration. Due to the narrow angular linewidth of the resonance used here (full-width at half-max = 0.3°) and because the optimal resonance angle shifts slightly higher with increasing spot density, the high-density spots are illuminated with a small angle offset from their true on-resonant state.

#136118 - $15.00 USD Received 6 Oct 2010; revised 5 Nov 2010; accepted 6 Nov 2010; published 11 Nov 2010

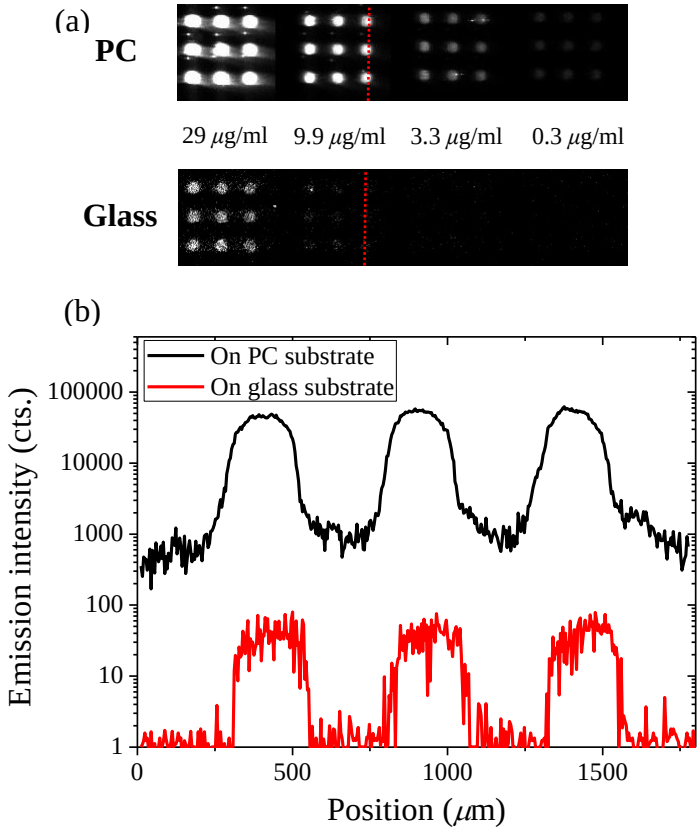

Fig. 9. (a) Gain and exposure-optimized images of PPL-Alexa 647 fluorescence on glass compared the PCEF surface; (b) Intensity profile as a function of distance for line of fluorescent image pixels profiling spots of concentration 9.9 *μg/ml* on both glass and the PCEF surface.

As a more appropriate performance metric for fluorescence-based assays (as opposed to raw intensity enhancement numbers), SNRs are calculated from the optimized images for each PPL-Alexa 647 concentration spotted onto the PC and glass slide and are shown in Fig. 10. The signal is background subtracted and noise is defined as the standard deviation of nine local background fluorescent spot intensities taken in each quadrant around the perimeter of each spot. The Limit of Detection (LOD) is defined as the concentration at which a SNR = 3 is obtained. SNR enhancement for the PC was found to be 330 × for the concentration (5 μg/ml) corresponding to the LOD on the glass slide. The LOD for the PC was found to be 35 ng/ml, which is 140 × times lower than that of the glass slide. The PC sensor will not only provide better SNR and lower LOD compared to glass but will also provide improved SNR and lower LOD when compared to an unpatterned quartz substrate. This is demonstrated by the enhancement in the signal due to extraction effect which will enhance the signal from the fluorophores on the PC surface and is independent of the excitation laser power.

#136118 - $15.00 USD Received 6 Oct 2010; revised 5 Nov 2010; accepted 6 Nov 2010; published 11 Nov 2010

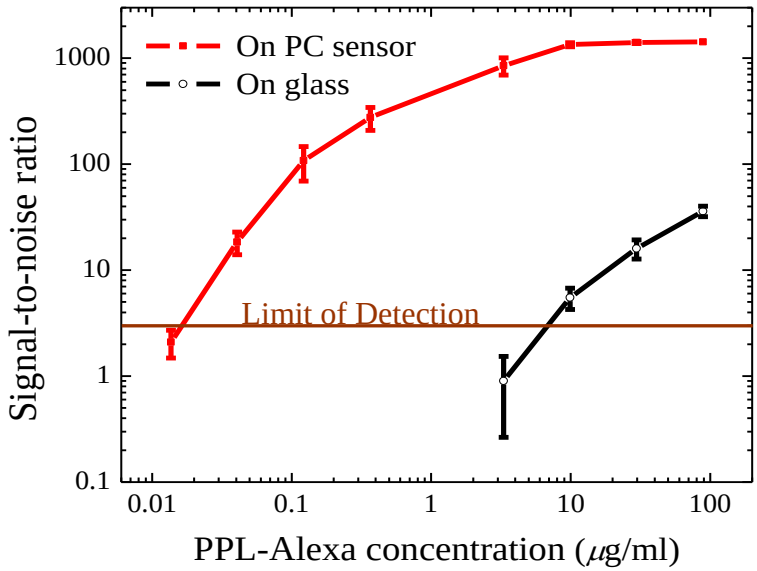

Fig. 10. Signal-to-noise vs PPL-Alexa 647 concentration showing an improvement in limit of detection (LOD) on a PCEF surface by a factor of 140.

Table 1. Measured Photonic Crystal Fluorescence Enhancement

[PPL-Alexa 647](μg/ml)	Enhanced Excitation*	Enhanced Extraction†	Total Enhancement‡
29 (On Res. PC saturates)	35	4	140
9.9	96	3	288
3.3	116	6	696
0.3 (Glass spots not visible)	131	–	–

* Net spot intensity for PC on resonance divided by net spot intensity for PC off resonance.
† Net spot intensity for PC off resonance divided by net spot intensity for glass control.
‡ Net spot intensity for PC on resonance divided by net spot intensity for glass control.

The difference in the measured maximum enhancement factors between detection of a dye-tagged polypeptide (696 ×) and a conformal thin film of dye-doped polymer (7500 ×) can be explained by several factors. Most importantly, the SU-8 film performs optically as a wave confinement layer with high refractive index relative to the air medium, which can hold a greater proportion of the resonant mode within its volume than biomolecule monolayers surrounded only by a low refractive index air medium. The SU-8 film is able to apply a conformal volume that is uniformly filled with dye, and that can partially fill the grating grooves, thus resulting in efficient overlap between the physical space occupied by dye molecules and the volume occupied by the resonant electric field. The peptide layer, in contrast, is confined to a two-dimensional monolayer film that can conform to the PC surface structure, but that does not occupy substantial volume. Characterization of the enhancement factor is presented here using both methods to facilitate comparison with approaches that primarily report results using only dye-doped polymer films.

We have observed that enhanced excitation using the PC has an effect of increasing the rate of the photobleaching of the fluorophores on the surface. However, it has been recently shown [50] that for all practical experimental time frames, the fluorescence signal for the PC

#136118 - $15.00 USD Received 6 Oct 2010; revised 5 Nov 2010; accepted 6 Nov 2010; published 11 Nov 2010

on-resonance will be higher than the fluorescence signal from an unpatterened glass substrate. Also, photobleaching is not an important issue for one-time scanning of DNA microarrays and protein microarrays.

6. Conclusions

This paper reports the design and fabrication of a PCEF surface that is fabricated upon a quartz substrate for low autofluorescence and high enhancement factors for simultaneous PC enhanced fluorophore excitation and PC enhanced fluorophore emission extraction. The PCEF surface gave a maximum enhancement factor of 7500 × for a ~50 nm thick layer of LD-700 (concentration of 538 ng/ml) doped SU-8 layer. Using dose-response characterization of deposited PPL-Alexa 647 spots of variable tagged molecule concentration, a SNR improvement of 330 × on the PC was demonstrated for the concentration corresponding to the LOD on an unpatterned glass surface. The LOD on the PC slide was lowered by 140 × compared to the LOD of PPL-Alexa on the glass control.

The PCEF surface can be used to provide lower detection limits for broad classes of surface-based fluorescent assays for applications that include DNA microarrays for quantification of gene expression, protein microarrays for detection of disease biomarkers in blood, and next-generation DNA sequencing applications that utilize fluorescent tags.

Acknowledgements

This work was supported by SRU Biosystems, the National Science Foundation (CBET 07-54122), and the National Institutes of Health (R01 GM086382). Any opinions, findings, and conclusions or recommendations expressed in this material are those of the authors and do not necessarily reflect the views of the National Science Foundation. The authors would like to thank Molecular Imprints, Inc. for their technical support. Contact * B.T. Cunningham, Tel: + 1-217-265-6291; bcunning@illinois.edu

#136118 - $15.00 USD Received 6 Oct 2010; revised 5 Nov 2010; accepted 6 Nov 2010; published 11 Nov 2010